Remapping annual precipitation in mountainous area based on vegetation pattern: a case study in the Nu River basin

Xing Zhou[1], Guang-Heng Ni[1], Chen Shen[1], Ting Sun[1]

1) State Key Laboratory of Hydro-Science and Engineering, Department of Hydraulic Engineering, Tsinghua University, Beijing 100084, China

Corresponding to: Ting Sun (sunting@tsinghua.edu.cn)

Abstract. Accurate high-resolution estimates of precipitation are vital to improve the understanding on basin-scale hydrology in mountainous areas. The traditional interpolation methods or satellite-based remote sensing products are known to have limitations in capturing spatial variability of precipitation in mountainous areas. In this study, we develop a fusion framework to improve the annual precipitation estimation in mountainous areas by jointly utilizing the gauge measured precipitation and vegetation index. The development consists of vegetation data merging, vegetation response establishment, and precipitation remapping. The framework is then applied to the mountainous area of Nu River basin for precipitation estimation. The results demonstrate the reliability of the framework in reproducing the high-resolution annual precipitation regime and capturing its high spatial variability in the Nu River basin. In addition, the framework can significantly reduce the errors in precipitation estimates as compared with the inverse distance weighted (IDW) method and TRMM (Tropical Rainfall Measuring Mission) precipitation product.

1 Introduction

Precipitation plays an important role in hydrological process, land-atmospheric processes, and ecological dynamics. Accurate high-resolution precipitation is crucial for streamflow prediction, flood control, and water resources management in data-sparse regions such as mountainous areas (Song et al., 2015). However, it is of great challenge to obtain accurate precipitation in mountainous areas due to the sparse gauge network and the remarkable spatiotemporal variability of precipitation. Conventional gauge networks can provide accurate precipitation measurements at point scales, which can be interpolated within the region of interest to give estimates of precipitation in ungauged areas. However, such interpolated estimates might not be reliable in mountainous areas considering the very limited gauges there (Phillips et al., 1992; Mair and Fares, 2011; Jacquin and Soto-Sandoval, 2013; Wang et al., 2014; Borges et al., 2016).

Recently, remote-sensing-based precipitation (RSBP) products, such as the Global Precipitation Climatology Project (GPCP) (Schamm et al., 2014), the Tropical Rainfall Measuring Mission (TRMM) (Council, 2005), and the Climate Prediction Center Morphing Method (CMORPH) (Joyce et al., 2004), have been extensively used in ungauged or sparsely-gauged areas to bridge the gap between the need for precipitation estimate and the scarcity in gauge observations (Akbari et al., 2012; Kneis et al., 2014; Li et al., 2015; Worqlul et al., 2015; Mourre et al., 2016; Wong et al., 2016). Also, data fusion across satellite and gauge observations is being conducted to further the application of RSBPs (Rozante et al., 2010; Woldemeskel et al., 2013; Arias-Hidalgo et al., 2013; Chen et al., 2016; Zhou et al., 2016). However, due to the relatively coarse spatial resolution (e.g., 0.25°–5°) and uncertainties of RSBPs, their applications in mountainous basins, where the precipitation shows large spatial variability, are still very limited (Krakauer et al., 2013; Chen and Li, 2016).

Precipitation estimates can be influenced by a variety of ambient factors (e.g., topography, vegetation, etc.). In order to correct effects of topography in precipitation estimate, Digital Elevation Model (DEM) has been widely used in spatial interpolation of precipitation over mountainous areas (Marquínez et al., 2003; Lloyd, 2005). However, the relationship between elevation and precipitation is not clear. Meanwhile, strong correlations between NDVI and precipitation are found by several studies (Li et al., 2002; Kariyeva and Van Leeuwen, 2011; Li and Guo, 2012; Sun et al., 2013; Campo-Bescós et al., 2013). As such, establishing statistical models between normalized difference vegetation index (NDVI) and precipitation so as to improve the spatial resolution of TRMM products in mountainous areas is becoming popular (Immerzeel et al., 2009; Jia et al., 2011; Duan and Bastiaanssen, 2013; Chen et al., 2014; Xu et al., 2015; Mahmud et al., 2015; Jing et al., 2016). For instance, Immerzeel et al. (2009) downscaled TRMM-3B43 to 1 km based on an exponential relationship between NDVI and TRMM precipitation in Iberian Peninsula of Europe. Jia et al. (2011) established four multivariable linear regression models between TRMM-3B43 precipitation and two other factors (i.e., DEM and NDVI) of different resolutions (0.25°, 0.5°, 0.75°, 0.1°) to get 1 km estimates of precipitation in the Qaidam Basin of China. Duan and Bastiaanssen (2013) used nonlinear relationship between TRMM-3B43 and NDVI to downscale precipitation to

1 km in a humid area and a semi-arid area. Chen et al. (2014) established spatially varying relationship among TRMM, NDVI, and DEM by using a local regression analysis approach known as geographically weighted regression (GWR) in South Korea. Xu et al. (2015) also used the GWR method to explore the spatial heterogeneity of the RSBP-NDVI and RSBP-DEM relationships over two mountainous area in western China.

However, the present RSBP-NDVI-based schemes have several limitations: 1) significant errors can be introduced during the downscaling given the nonlinear relationship between RSBP and NDVI; 2) large uncertainties exist in the RSBP for mountainous areas, and 3) inter-comparison of existing NDVI datasets are missing in deriving the RSBP-NDVI relationships. In this study, we develop a fusion framework to obtain more accurate high-resolution estimates of annual precipitation in mountainous areas based on the relationship between precipitation and vegetation response. More specifically, in addition to RSBP, gauge measurements and different vegetation datasets will be used in this study to overcome the aforementioned limitations in current RSBP-NDVI-based schemes. The paper is organized as follows: section 2 describes the development of the fusion framework; section 3 documents the study area and related datasets; section 4 presents the results of the fusion framework and discusses impacts of different determinants on the performance of fusion framework; and section 5 summarizes this work.

2 Framework development

The satellite-gauge-vegetation fusion framework (Fig. 1) involves three stages of development: 1) vegetation data merging, 2) precipitation-vegetation regression, and 3) RSBP product remapping, whose details are described in the following subsections.

2.1 vegetation data merging

Vegetation closely interacts with soil moisture and is recognized as a good proxy of precipitation. The remote sensing technique provides us with various high-resolution vegetation products such as NDVI, EVI (enhanced vegetation index), LAI (leaf area index), etc. Among the vegetation indices, NDVI, an indicator of plant density and growth, is chosen as the proxy of precipitation in this study due to its wide availability. Considering the crucial role of NDVI in deriving precipitation estimates under our framework, we conduct an inter-comparison in data accuracy between two NDVI datasets (termed as datasets A and B hereinafter) to reduce the error. First, the systematic errors of both datasets are eliminated by multiplying reduction factor or using simple regression model. After the correction, the final dataset is then obtained by selecting better element between A and B if the quality criteria is satisfied otherwise filling an anomaly value.

It should be noted that since the vegetation growth is suppressed or promoted on some land covers (e.g. rivers, lakes, snow and ice, and urban areas), the vegetation data of these land covers are excluded by filling anomaly values. Besides, due to the strong influence of farming activities (e.g. irrigation, fertilization, and harvest) on the crop growth, vegetation data of farmland are excluded as well. We note that although Moran's Index (Li et al., 2007) is widely employed to detect anomalies in vegetation data (Jia et al., 2011; Duan et al., 2013), it is not used in this study for its inapplicability in large areas with continuous anomaly pixels (e.g. farmland). As such, we identify anomaly pixels simply by landuse type: pixels categorized as water, wetland, urban, cropland, snow/ice, and barren will be identified as anomalies. The detected anomaly pixels are excluded from the original NDVI dataset and then filled with interpolated values using IDW method so as to generate an optimized NDVI dataset.

Based on the optimized NDVI dataset, the NDVI data at the gauge locations are retrieved with neighbor-average method (i.e. the value of a certain grid is determined as the average of the grid and the eight neighboring grids) and will be used for the precipitation-vegetation regression.

2.2 precipitation-vegetation regression

As far as we know, there is no widely accepted form for the precipitation-vegetation relationship. Therefore, the final regression form will be determined from several candidate relationships, including polynomial, exponential, logarithmic and linear forms, according to the five metrics: correlation coefficient (R), coefficient of determination (R^2), root-mean-square error (E_{RMS}), mean relative error (E_{MR}) and mean absolute relative error (E_{MAR}), which are given as follows:

$$R = \frac{\sum_{i=1}^{n}(P_i - \bar{P})(O_i - \bar{O})}{\sqrt{\sum_{i=1}^{n}(P_i - \bar{P})^2}\sqrt{\sum_{i=1}^{n}(O_i - \bar{O})^2}} \quad (1)$$

$$R^2 = \frac{\sum_{i=1}^{n}(P_i - O_i)^2}{\sqrt{\sum_{i=1}^{n}(O_i - \bar{O})^2}} \quad (2)$$

$$\mathrm{E}_{\mathrm{RMS}} = \sqrt{\frac{\sum_{i=1}^{n}(P_i - O_i)^2}{n}} \quad (3)$$

$$\mathrm{E}_{\mathrm{MR}} = \frac{1}{n}\sum_{i=1}^{n}(P_i - O_i) \quad (4)$$

$$\mathrm{E}_{\mathrm{MAR}} = \frac{1}{n}\sum_{i=1}^{n}\frac{|P_i - O_i|}{O_i} \quad (5)$$

where $\overline{O}$ is the mean annual precipitation of all gauges, O_i the mean annual precipitation of gauge *i*, P_i the estimated precipitation at gauge *i*, and *n* the total number of gauges.

Also, considering the annual variability of precipitation, the regression model is further determined for two temporal scales: 1) entire period covering all the study years and 2) individual year of the entire study period. The **R**egression **M**odels for **E**ntire study period and for **I**ndividual years are thus termed as **RME** and **RMI**, respectively. RME can utilize the full knowledge of precipitation characteristics of the entire study period, whereas RMI implies the inter-annual variability. Besides, RME can reasonably reconstruct the precipitation series of the years when data gaps exist.

The calibration-validation procedure for each candidate model is conducted under three scenarios with different numbers of gauge and/or years:

a) Fully random: random number of gauges and random number of years are independently used for calibration and validation;
b) All gauges, partial period: all the gauges will be involved in both procedures, but only 2/3 of years will be randomly chosen for calibration and the other years for validation;
c) Partial gauges, entire period: all years will be used, but only 1/3 of gauges will be randomly chosen for calibration and other gauges for validation.

For each scenario, the calibration-validation procedure will be performed for one hundred samples determined based on the above criteria and the six evaluation metrics (i.e. R, R^2, $\mathrm{E}_{\mathrm{RMS}}$, E_{MA} and $\mathrm{E}_{\mathrm{MAR}}$) will be calculated for each sample accordingly. The best model is then determined based the metrics.

2.3 RSBP product remapping

With the optimized vegetation dataset and precipitation-vegetation regression model, the RSBP product is then remapped over the study region. Thanks to the finer resolution of NDVI dataset than RSBP product and the accurate estimate of precipitation by gauges, the remapped RSBP product is expected to provide more detailed spatial characteristics of precipitation over mountainous areas.

3 Study area and datasets for framework application

3.1 Study area

The Nu-Salween basin (Fig. 2a), where 6 million people are living, is one of the largest river basins in South Asia and spreads across three countries with an area of 324,000 km^2. This study focuses on the Chinese part of the Nu-Salween basin (termed as the Nu river basin hereafter), where the elevation ranges from 446 m to 6134 m and the narrowest part is only 24 km. The annual precipitation of the Nu river basin ranges from 400 mm to 2000 mm with an average of 900 mm and the mean annual runoff is 69 km^3. The precipitation of the Nu river basin generally decreases from southwest to northeast and demonstrates high variability due to mountain weather systems (e.g. the difference in annual precipitation between the mountaintop and valley of Gongshan is larger than 1000 mm). Precipitation during the year across this region varies significantly. Fig. 2b shown the distributions of precipitation during the year for 7 stations located in up, middle and downstream of Nu River. The upstream and downstream have similar distribution of precipitation with major precipitation occurs in summer and little occurs in winter while the middle of Nu River has relatively large precipitation in winter and spring. Thanks to the adequate precipitation and minimal human perturbation, the Nu river basin has an extensive vegetation coverage with the dominant type as grassland in the Qinghai-Tibetan Plateau (upper basin) and mixed forest in Yunnan province (lower basin). However, the dense vegetation cover increases the difficulty in conducting precipitation observations and only 13 gauges are very unevenly distributed over the whole basin of 142,479 km^2, which makes it highly challenging to obtain the accurate spatial precipitation characteristics with traditional interpolation approaches. Although the RSBP products are available for this area, they are too course (usually with a spatial resolution of ~50 km) to capture the high spatial variability of precipitation.

Considering the limited number of gauges (i.e. 13) in the Nu river basin, an enlarged area covering 23°N–33°N and 91°E–101°E is chosen for the application of the fusion framework, where 59 gauges are available and the climatic and topographic conditions are similar: both regions are characterized as mountainous areas under the subtropical climate influenced by southeast and southwest monsoons. Besides, given no rain gauges are available outside of China in this study region, the non-Chinese region is excluded from the study area.

3.2 Datasets

3.2.1 Vegetation data

In this study, we use two MODIS (moderate resolution imaging spectoradiometer) vegetation products, MOD13A3 (termed MOD hereafter) and MYD13A3 (termed MYD hereafter), in the application of the fusion framework. Both the MOD and MYD datasets contain 10 sub-datasets consisting of NDVI, EVI and pixel reliability. The temporal and spatial resolutions of the MOD13A3 and MYD13A3 products are 1 month and 1 km, respectively. The pixel reliability is an accuracy metric of the data quality pixel and has four valid values: 0 for good reliability, 1 for marginal reliability, 2 for snow/ice, and 3 for cloud. Based on the pixel reliability information, the NDVI values are either selected for corresponding pixel reliability levels being 0 and 1 or discarded as anomalies otherwise.

The MOD dataset is used as benchmark while MYD is taken as the alternative for occasions when MOD data are missing or have large uncertainties. Since both the MOD and MYD datasets are extracted from different satellites at different transit times, systematic errors may exist in the difference between the two datasets. As such, we construct two regressions to remove their systematic errors: one is based on a subset with both MOD and MYD of good reliability (= 0), and the other on a subset with MOD of marginal reliability (= 1) and MOD of good reliability (= 0). After the removal of systematic errors, a merged dataset of MOD and MYD (termed MMD hereafter) is generated under the criteria given as follows:

$$MMD = \begin{cases} MOD & (MOD == 0) \\ MYD & (MOD > 1\ \& MYD == 0) \\ MOD & (MOD == 1\ \& MYD == 1) \\ NULL & (MOD > 1\ \& MYD > 0) \end{cases} \tag{6}$$

The annual MMD dataset is then calculated by averaging the 12 monthly images.

3.2.2 Landuse data

The landuse dataset MCD12Q1 Version 51 (MODIS/Terra+Aqua Land Cover Type Yearly L3 Global 500m SIN Grid V051) in period of 2001-2013 is used to identify the anomalies of MMD, while the IGBP (International Geosphere Biosphere Programme) classification is adopted for its wide applications. Due to mismatch in spatial resolutions between MMD and MCD12Q1 datasets, the MCD12Q1 dataset is upscaled to 1km as MMD for anomaly identification. It should be noted that if any of the four 500 m pixels in MCD12Q1 classified as water, urban, snow/ice and cropland, the upscaled 1 km pixel will be classified as anomalous pixel (or non-natural vegetation) and assigned with a missing value (i.e. -9999), otherwise will be classified as normal pixel (or natural vegetation) and assigned with a 1 value.

3.2.3 Weather data

Datasets consisting of daily precipitation and air temperature collected at the 59 gauges in the study area are obtained via the China Meteorological Data Sharing Service system (http://data.cma.cn/data/detail/dataCode/SURF_CLI_CHN_MUL_DAY_V3.0/keywords/v3.0.html). The air temperature measurements will be used for dependence analysis later in Section 4.5. The streamflow data provided by Yunnan University will be used for calculating sub-basin scaled precipitation based on water balance. The 5 hydrological stations are Gongshan, Liuku, Jiucheng, Gulaohe and Dawanjiang with the drainage area of 101146, 106681, 6308, 4185 and 7986 km^2, respectively. MODIS evapotranspiration (ET) product MOD16 (http://www.ntsg.umt.edu/project/mod16) with the spatiotemporal resolution of 1 km/1 weekly will also be used in calculating precipitation based on water balance.

4 Results and discussion

4.1 Model calibration and validation

Based on the results of six evaluation metrics for different regression form candidates (Fig. 3a), the 2nd-order polynomial is chosen as the regression model form in this study:

$$p = a\,NDVI^2 + b\,NDVI + c \qquad (7)$$

where p denotes precipitation amount in mm, and a, b and c are regression coefficients. The results of regression coefficients and evaluation metrics are given in Table 1, and the precipitation-NDVI relationships for the study period are demonstrated in Fig. 3b.

The best performance of the regression model is found within $0.2 < NDVI < 0.7$ and 400 mm $year^{-1} < p < 1500$ mm $year^{-1}$. Larger errors are found at pixels with NDVI larger than 0.7 or annual precipitation larger than 1500 mm, implying the water supply is no longer a determinant of vegetation growth as annual precipitation exceeds a certain threshold.

In general, the RMIs demonstrate better performance than RME, which can be attributable to the less variability of precipitation in a single year than the whole study period. It is also noted that the R^2 values of RMIs for drier years (2003, 2009 and 2011) are less than wetter years, indicating the weaker coupling effect between vegetation growth and precipitation.

The performance of regression models is assessed under three scenarios as described in Section 2.2. A total of 300 tests are conducted and performance metrics (i.e., R, R^2, E_{RMS}, and E_{MAR}) are calculated accordingly (Fig. 4 and Table 2). The high R values (> 0.85) indicate a strong correlation between NDVI and precipitation independent of sampling method. Also, the regression models demonstrate good performance with R^2 larger than 0.75 and E_{MAR} less than 20%. In addition, the metrics of regression models fluctuate around that of the RME with narrow inter-quartile ranges, indicating the regression models have remarkable consistency with the RME model.

Scenario a is designed to examine inter-annual stability in the performance of regression models, where the good performance indicates the acceptable ability of the RME model in estimating precipitation during periods when precipitation measurements are not available. Scenarios b and c investigate the impacts of spatial and temporal coverages of measurements, respectively. It is noteworthy that under scenario b better performance in regression models is observed as compared with scenario c, implying greater importance of spatial coverage of measurements in conducting the regressions. In addition, the results of calibration is better than validation as revealed by all metrics criterions as expected. However, the differences between calibration and validation are not significant, implying the consistent performance of regression models under various scenarios.

The performance of RME is further assessed by comparing the estimates against observations (Fig. 5), and good agreement between estimates and observations is observed. It should be noted the RME shows difficulty in estimating precipitation larger 2000 mm (cf. the dashed line in Fig. 5), implying the limitation of the fusion framework inherited from the oversaturation effect of vegetation index.

Elevation effect on the relationship between precipitation and NDVI is a concern to appreciate. An overall negative relationship is found between precipitation and elevation for the whole elevation range (i.e., 0–5000 m) with a R^2 value of 0.62 (Fig. 6a), whereas there is only unapparent/weak relationship at different elevation bands (Fig. 6b-f). Given the spatial heterogeneity of orographic effects on precipitation (Brunsdon et al., 2001; Daly et al., 2008) and insufficient data of this study, a more thorough investigation of the relationship between precipitation and elevation needs to be conducted with more information that might be available in the future. Positive precipitation-NDVI relationships are found at different elevation bands (Fig. 7) with the best and worst fitness observed at elevation band 2000–3500 m with a R^2 value of 0.94 and at elevation band 0–2000 m with a R^2 value of 0.62, respectively. By comparing the three regressions at different bands with the global regression, we notice that more significant overestimates of precipitation are observed with the range of lower NDVI values (<0.4) at band 0–2000 m than other three regressions whereas regression at band >3500 m has a significant overestimation of precipitation than other three regressions for higher NDVI values (>0.5).

4.2 Spatial characteristics of precipitation

The spatial characteristics of precipitation of the study area are investigated with RME for the whole study period (Fig. 8). Annual precipitation in Nu River is observed to decrease from south to north and from west to east with prominent spatial variability. Two "hot-spot" regions, whose annual precipitation exceeds 1500 mm, can be identified in the study areas: one near south border and the other close to southwestern mountain border. The east part of the Nu river basin featuring a dry and warm climate receives an average annual precipitation of 800 mm with large inter-annual variability. A precipitation product based on precipitation-elevation relationship (DEMP) is used to compare with RME. There is no obvious distribution pattern of precipitation (Fig.9a) and a smaller spatial variability compared to RME in the DEMP product, indicating the advantage of RME in representing the spatial variability of annual precipitation. And the overall underestimation of precipitation is observed in the DEMP product across the whole study area (Fig.9b). In addition, the pixels in Fig.8 with a value out of the valid range (i.e., 400 mm/yr < P< 1500 mm/yr) may have relatively large error as discussed in section 4.1. As there is no justifiable methods for such correction and given the limited fraction of invalid pixels (10% in the whole study area and 7% in the Nu River basin), the figure can be used to demonstrate a full picture of the spatial precipitation pattern in the study area, but we note those pixels are of large uncertainties and should be interpreted with caution.

4.3 Model performance comparison

The performance between IDW approach, TRMM product and the fusion framework is compared in this section. IDW is one of the most popular methods for spatial interpolation of precipitation due to its easy implementation and flexibility in incorporating other auxiliary information (e.g., elevation). In general, the IDW approach is unable to demonstrate the high spatial variability though it can capture the general spatial distribution of whole basin (Fig. 10a) as TRMM (Fig. 10b). Due to the coarse spatial resolution, TRMM cannot capture the high variability in the river valley where the elevation varies significantly. Although large precipitation (>1800mm) is observed in both our and TRMM products in the southwest of the study area region, our product gives lower precipitation compared to TRMM. As discussed above, the regression model tends to underestimate precipitation as the annual precipitation exceeds a certain threshold because the water supply is no longer a determinant of vegetation growth.

To demonstrate the advantage of the fusion framework, a cross-validation is conducted against the randomly sampled gauge observations by varying the number of samples (1 - 40). The cross-validation shows higher E_{RMS} for the IDW approach, followed by TMMM and RME (Fig. 11a). A higher mean E_{MR} of 15% is observed for TRMM than IDW (8%) and RME (5%) while the difference in E_{MAR} are minimal between TRMM and IDW. The results indicate an overestimated precipitation by TRMM as compared to gauge observations. Table 3 summarizes the maximum, minimum and mean values of each method and shows the relative difference between RME and other two methods. On average, E_{RMS} of RME is smaller than that of IDW and TRMM by 20.4% and 17.4%, respectively. In general, the fusion framework demonstrates better performance than the other approaches.

To further evaluate the performance of RME, the annual averages of precipitation of five hydrological stations (Fig. 12a) and whole basin estimated by the three approaches (IDW, RME and TRMM) are compared. At the whole basin scale, the estimate by RME is 5.2% higher than that of IDW while 7.9% lower than TRMM. Although the difference between the three approaches is minimal at the basin scale, the difference at the sub-basin scale is remarkable. In the upstream region (i.e., Gongshan sub-basin) located in Tibet Plateau, TRMM overestimates precipitation by 13.2% while IDW underestimates by 7.6% as compared with RME. In the other four downstream sub-basins, estimates by RME are larger than those by IDW and TRMM. In general, in the midstream and downstream regions with large variability in terrain height, RME gives larger estimates of precipitation than IDW and TRMM.

To evaluate the accuracy of different precipitation estimates, we utilize MODIS evapotranspiration product MOD16 to calculate water balance based precipitation (i.e. ET+R). Then we compare it with 5 precipitation products including RME, BandP (precipitation based on precipitation-NDVI relationship with consideration of elevation band), DEMP, TRMM, IDW (Fig.12b). It can be found that RME and BandP produce closer estimation to water balance based precipitation, implying that the precipitation mapping result based on precipitation-NDVI relationship is reasonable.

We also compared our products with the Multi-Source Weighted-Ensemble Precipitation (MSWEP) product. The dataset takes advantage of a wide range of data sources, including gauges, satellites, and atmospheric reanalysis models, to obtain the best possible precipitation estimates at global scale with a high 3-hourly temporal and 0.25° spatial resolution (Beck et al., 2016). Comparison in the annual mean precipitation between the gauge measurements and predictions by the MSWEP and TRMM product (Fig. 13) shows acceptable performance of both MSWEP and TRMM in predicting the precipitation with an overall overestimation. The RMSE values for MSWEP, TRMM and RME are 241 mm, 196 mm, and 174 mm, respectively, indicating that RME gives the best prediction among the three products. The possible reason why MSWEP shows no superiority over TRMM in predicting annual precipitation is that very few gauges are available in this region that might limit the applicability of MSWEP method. However, the MSWEP method does provide insights into the production of high temporal resolution (3-hourly) precipitation, which we believe will be helpful to our future work.

4.4 influence of different vegetation index

Considering the possible degradation in model performance caused by oversaturation of NDVI in high biomass areas, another vegetation indicator, Enhanced Vegetation Index (EVI), is suggested as an alternative for estimating vegetation growth (Matsushita et al., 2007; Liao et al., 2015). As such, we also test the fusion framework with EVI in addition to NDVI and the results are assessed against the gauge observations.

Based on the chosen metrics, EVI is found to outperform NDVI with better regression quality (Table 4): EVI-based regression model gives higher R^2, smaller E_{RMS} and E_{MAR} compared to the NDVI-based model. Also, remarkable difference is observed in the precipitation estimates based on the two vegetation indices (Fig. 14). It is noted that the curvature of EVI-based model is larger than NDVI-based model, suggesting higher sensitivity of EVI-based model in humid environment. Although the EVI-based model demonstrates better performance than the NDVI-based one, it should be noted that NDVI is the most popular vegetation index used in operational applications among the available vegetation index products. Besides, NDVI has a relative longer temporal coverage compared to other vegetation index products. For instance, the AVHRR (Advanced Very High Resolution Radiometer) NDVI data are available since 1982 with a global coverage. As such, under scenarios when EVI is unavailable, NDVI is a satisfactory index that can be used in the fusion framework.

4.5 Influence of other ambient determinants

One major assumption of the proposed framework is that precipitation is the only determinant of vegetation growth and thus NDVI is regarded as a proxy for precipitation. However, other ambient factors, such as soil properties, solar radiation, air temperature, elevation, etc., may significantly influence the vegetation growth as well as NDVI values. Considering the data availability of various ambient factors, air temperature and elevation, in addition to NDVI, are adopted as extra determinants to establish the regression models, which are thus termed as RME+T and RME+H for air temperature and elevation, respectively. We note that for simplicity, the extra determinants are assumed to have linear relationship with precipitation.

The difference in R^2, E_{RMS}, and E_{MAR} between the three models are minimal and the regression coefficients of the three models are very close to each other (Table 5). The negative regression coefficient of temperature in RME+T indicates inconsistent trends between precipitation and temperature. Since the temperature decreases with the increase in elevation, RME+T and RME+H essentially provides consistent estimates of precipitation which is also clearly shown in Fig. 15. It is also noted the added information by extra determinants (i.e., air temperature and elevation) is in fact minimal. Overall there is little difference between RME and other two products. Therefore, we consider the RME-only based vegetation index as a simple and efficient model for precipitation estimation.

5 Conclusion

In this study, a satellite-gauge-vegetation fusion framework has been developed for estimating the precipitation in mountainous areas by establishing regression relationship between gauge-based precipitation observations and satellite-based vegetation dataset. The fusion framework was then applied in the Nu River basin of Southwest China for estimating precipitation between 2001 and 2012.

The fusion framework for the Nu River basin adopted a second order polynomial form and demonstrated promising ability in capturing the high spatial variability of precipitation in the river valley. Six evaluation metrics, including R, R^2, E_{RMS}, E_{MR} and E_{MAR}, indicated good performance of the fusion framework in precipitation estimation. The performance of the fusion framework was also compared with the IDW approach and TRMM product and the comparison results indicated that the fusion framework generally outperformed other approaches in estimating precipitation in mountainous areas. On average, the E_{RMS} of the fusion framework is 20.4%, 17.4% smaller than that of IDW and TRMM, respectively. E_{MR} of the fusion framework is 1.2%, 71.5% smaller than that of IDW and TRMM. E_{MAR} the fusion framework is 18.9%, 28.3% smaller than that of IDW and TRMM.

The success of application of the fusion framework in the Nu River sheds light on the precipitation estimation in mountainous areas by using multi-source datasets. However, this framework does have certain limitations that are important to appreciate. First, the framework is applied only in the Nu River basin. More mountainous areas under different climates need to be examined to further test the robustness of this framework. In addition, although the RME model can utilize the full knowledge of precipitation in the entire study period compared with RMI models, the difference in the coefficients suggests apparent inter-annual variability of precipitation that should be considered when applying these models. Given the duration of study period and purpose, we suggest the RME model be used for long-term climatology identification while RMI models for inter-annual variability examination. Also, to fully verify the theoretical basis of this framework that vegetation actively interacts with precipitation in mountainous areas, future work is required to refine the spatiotemporal resolution of this study to enable better scrutiny into vegetation-precipitation interactions at sub-monthly scales across more detailed vegetation species.

Acknowledgments

The study is supported by NSFC under grant U1202231, 51679119 and 91647107, National Key Technology Support Program under grant 2011BAC09B07-3 and by China Postdoctoral Science Foundation under grant 2015T80093. The authors thank China Meteorological Administration, Yunnan University, MODIS NDVI, Tropical Rainfall Measuring Mission (TRMM) and the Shuttle Radar Topography Mission (SRTM) for providing the data used in this study.

Appendix: Merging of NDVI datasets

The merging of NDVI datasets improves the accuracy as expected (Fig. A1), the monthly error rates (i.e., the ratio of the pixel which quality value is over 1) of MOD and MMD are generally reduced with an average of 5% and over 20% in several months. Fig.A2 shows that the accuracy of MMD is significantly improved in a ridge area covering 23°10′ N–23°40′ N and 98°30′ E–99°E. Fig. A2b shows NDVI value near right and left boundary is underestimated by MOD. Fig.A2c shows NDVI value in the middle boundary is underestimated by MYD. The underestimates in both products near the boundary of MOD and MYD are amended (Fig. A2a). Fig.A3 shows the three NDVI series for one rain gauge. Comparing with MOD series, the improved accuracy in MMD is mainly observed in the wet season (from May to October), when the NDVI values could be often underestimated due to the overcasts.

References

Akbari, A., Abu Samah, A. and Othman, F.: Integration of SRTM and TRMM date into the GIS-based hydrological model for the purpose of flood modelling, Hydrol Earth Syst Sci Discuss, 2012, 4747–4775, doi:10.5194/hessd-9-4747-2012, 2012.

Borges, P. de A., Franke, J., Anunciação, Y. M. T. da, Weiss, H. and Bernhofer, C.: Comparison of spatial interpolation methods for the estimation of precipitation distribution in Distrito Federal, Brazil, Theor. Appl. Climatol., 123(1–2), 335–348, doi:10.1007/s00704-014-1359-9, 2016.

Beck, H.E., A.I.J.M. van Dijk, V. Levizzani, J. Schellekens, D.G. Miralles, B. Martens, A. de Roo (2016): MSWEP: 3-hourly 0.25° global gridded precipitation (1979–2015) by merging gauge, satellite, and reanalysis data, Hydrology and Earth System Sciences Discussions, doi:10.5194/hess-2016–236.

Brunsdon, C., McClatchey, J. and Unwin, D. J.: Spatial variations in the average rainfall-altitude relationship in Great Britain: an approach using geographically weighted regression, Int. J. Climatol., 21, 455–466, doi:10.1002/joc.614, 2001.

Campo-Bescós, M. A., Muñoz-Carpena, R., Southworth, J., Zhu, L., Waylen, P. R. and Bunting, E.: Combined

Spatial and Temporal Effects of Environmental Controls on Long-Term Monthly NDVI in the Southern Africa Savanna, Remote Sens., 5(12), 6513–6538, doi:10.3390/rs5126513, 2013.

Chen, F. and Li, X.: Evaluation of IMERG and TRMM 3B43 Monthly Precipitation Products over Mainland China, Remote Sens., 8(6), 472, doi:10.3390/rs8060472, 2016.

Chen, F., Liu, Y., Liu, Q. and Li, X.: Spatial downscaling of TRMM 3B43 precipitation considering spatial heterogeneity, Int. J. Remote Sens., 35(9), 3074–3093, doi:10.1080/01431161.2014.902550, 2014.

Chen, J., Yong, B., Ren, L., Wang, W., Chen, B., Lin, J., Yu, Z. and Li, N.: Using a Kalman Filter to Assimilate TRMM-Based Real-Time Satellite Precipitation Estimates over Jinghe Basin, China, Remote Sens., 8(11), 899, doi:10.3390/rs8110899, 2016.

Council, N. R.: Assessment of the Benefits of Extending the Tropical Rainfall Measuring Mission: A Perspective from the Research and Operations Communities, Interim Report. [online] Available from: https://www.nap.edu/catalog/11195/assessment-of-the-benefits-of-extending-the-tropical-rainfall-measuring-mission (Accessed 18 November 2016), 2005.

Daly, C., Halbleib, M., Smith, J. I., Gibson, W. P., Doggett, M. K., Taylor, G. H., Curtis, J. and Pasteris, P. P.: Physiographically sensitive mapping of climatological temperature and precipitation across the conterminous United States, Int. J. Climatol., 28, 2031–2064, doi:10.1002/joc.1688, 2008.

Duan, Z. and Bastiaanssen, W. G. M.: First results from Version 7 TRMM 3B43 precipitation product in combination with a new downscaling–calibration procedure, Remote Sens. Environ., 131, 1–13, doi:10.1016/j.rse.2012.12.002, 2013.

Huffman, G. J., Adler, R. F., Arkin, P., Chang, A., Ferraro, R., Gruber, A., Janowiak, J., McNab, A., Rudolf, B. and Schneider, U.: The Global Precipitation Climatology Project (GPCP) Combined Precipitation Dataset, Bull. Am. Meteorol. Soc., 78(1), 5–20, doi:10.1175/1520-0477(1997)078<0005:TGPCPG>2.0.CO;2, 1997.

Immerzeel, W. W., Rutten, M. M. and Droogers, P.: Spatial downscaling of TRMM precipitation using vegetative response on the Iberian Peninsula, Remote Sens. Environ., 113(2), 362–370, doi:10.1016/j.rse.2008.10.004, 2009.

Jacquin, A. P. and Soto-Sandoval, J. C.: Interpolation of monthly precipitation amounts in mountainous catchments with sparse precipitation networks, Chil. J. Agric. Res., 73(4), 406–413, doi:10.4067/S0718-58392013000400012, 2013.

Jia, S., Zhu, W., Lű, A. and Yan, T.: A statistical spatial downscaling algorithm of TRMM precipitation based on NDVI and DEM in the Qaidam Basin of China, Remote Sens. Environ., 115(12), 3069–3079, doi:10.1016/j.rse.2011.06.009, 2011.

Jing, W., Yang, Y., Yue, X. and Zhao, X.: A Spatial Downscaling Algorithm for Satellite-Based Precipitation over the Tibetan Plateau Based on NDVI, DEM, and Land Surface Temperature, Remote Sens., 8(8), 655, doi:10.3390/rs8080655, 2016.

Joyce, R. J., Janowiak, J. E., Arkin, P. A. and Xie, P.: CMORPH: A Method that Produces Global Precipitation Estimates from Passive Microwave and Infrared Data at High Spatial and Temporal Resolution, J. Hydrometeorol., 5(3), 487–503, doi:10.1175/1525-7541(2004)005<0487:CAMTPG>2.0.CO;2, 2004.

Kariyeva, J. and Van Leeuwen, W. J. D.: Environmental Drivers of NDVI-Based Vegetation Phenology in Central Asia, Remote Sens., 3(2), 203–246, doi:10.3390/rs3020203, 2011.

Kneis, D., Chatterjee, C. and Singh, R.: Evaluation of TRMM rainfall estimates over a large Indian river basin (Mahanadi), Hydrol Earth Syst Sci, 18(7), 2493–2502, doi:10.5194/hess-18-2493-2014, 2014.

Krakauer, N. Y., Pradhanang, S. M., Lakhankar, T. and Jha, A. K.: Evaluating Satellite Products for Precipitation Estimation in Mountain Regions: A Case Study for Nepal, Remote Sens., 5(8), 4107–4123, doi:10.3390/rs5084107, 2013.

Li, B., Tao, S. and Dawson, R. W.: Relations between AVHRR NDVI and ecoclimatic parameters in China, Int. J. Remote Sens., 23(5), 989–999, doi:10.1080/01431160110070690, 2002.

Li, D., Ding, X. and Wu, J.: Simulating the regional water balance through hydrological model based on TRMM satellite rainfall data, Hydrol Earth Syst Sci Discuss, 2015, 2497–2525, doi:10.5194/hessd-12-2497-2015, 2015.

Li, H., Calder, C. A. and Cressie, N.: Beyond Moran's I: Testing for Spatial Dependence Based on the Spatial Autoregressive Model, Geogr. Anal., 39(4), 357–375, doi:10.1111/j.1538-4632.2007.00708.x, 2007.

Li, Z. and Guo, X.: Detecting Climate Effects on Vegetation in Northern Mixed Prairie Using NOAA AVHRR 1-km Time-Series NDVI Data, Remote Sens., 4(1), 120–134, doi:10.3390/rs4010120, 2012.

Liao, Z., He, B. and Quan, X.: Modified enhanced vegetation index for reducing topographic effects, J. Appl. Remote Sens., 9(1), 096068–096068, doi:10.1117/1.JRS.9.096068, 2015.

Lloyd, C. D.: Assessing the effect of integrating elevation data into the estimation of monthly precipitation in Great Britain, J. Hydrol., 308(1–4), 128–150, doi:10.1016/j.jhydrol.2004.10.026, 2005.

Mahmud, M. R., Numata, S., Matsuyama, H., Hosaka, T. and Hashim, M.: Assessment of Effective Seasonal Downscaling of TRMM Precipitation Data in Peninsular Malaysia, Remote Sens., 7(4), 4092–4111, doi:10.3390/rs70404092, 2015.

Mair, A. and Fares, A.: Comparison of Rainfall Interpolation Methods in a Mountainous Region of a Tropical Island, J. Hydrol. Eng., 16(4), 371–383, doi:10.1061/(ASCE)HE.1943-5584.0000330, 2011.

Marquínez, J., Lastra, J. and García, P.: Estimation models for precipitation in mountainous regions: the use of GIS and multivariate analysis, J. Hydrol., 270(1–2), 1–11, doi:10.1016/S0022-1694(02)00110-5, 2003.

Matsushita, B., Yang, W., Chen, J., Onda, Y. and Qiu, G.: Sensitivity of the Enhanced Vegetation Index (EVI) and Normalized Difference Vegetation Index (NDVI) to Topographic Effects: A Case Study in High-density Cypress Forest, Sensors, 7(11), 2636–2651, doi:10.3390/s7112636, 2007.

Mourre, L., Condom, T., Junquas, C., Lebel, T., E. Sicart, J., Figueroa, R. and Cochachin, A.: Spatio-temporal assessment of WRF, TRMM and in situ precipitation data in a tropical mountain environment (Cordillera Blanca, Peru), Hydrol Earth Syst Sci, 20(1), 125–141, doi:10.5194/hess-20-125-2016, 2016.

Phillips, D. L., Dolph, J. and Marks, D.: A comparison of geostatistical procedures for spatial analysis of precipitation in mountainous terrain, Agric. For. Meteorol., 58(1), 119–141, doi:10.1016/0168-1923(92)90114-J, 1992.

Schamm, K., Ziese, M., Becker, A., Finger, P., Meyer-Christoffer, A., Schneider, U., Schröder, M. and Stender, P.: Global gridded precipitation over land: a description of the new GPCC First Guess Daily product, Earth Syst. Sci. Data, 6(1), 49–60, doi:10.5194/essd-6-49-2014, 2014.

Song, J., Xia, J., Zhang, L., Wang, Z.-H., Wan, H. and She, D.: Streamflow prediction in ungauged basins by regressive regionalization: a case study in Huai River Basin, China, Hydrol. Res., nh2015155, doi:10.2166/nh.2015.155, 2015.

Sun, J., Cheng, G., Li, W., Sha, Y. and Yang, Y.: On the Variation of NDVI with the Principal Climatic Elements in the Tibetan Plateau, Remote Sens., 5(4), 1894–1911, doi:10.3390/rs5041894, 2013.

Wang, S., Huang, G. H., Lin, Q. G., Li, Z., Zhang, H. and Fan, Y. R.: Comparison of interpolation methods for estimating spatial distribution of precipitation in Ontario, Canada, Int. J. Climatol., 14(34), 3745–3751, doi:10.1002/joc.3941, 2014.

Woldemeskel, F. M., Sivakumar, B. and Sharma, A.: Merging gauge and satellite rainfall with specification of associated uncertainty across Australia, J. Hydrol., 499, 167–176, doi:10.1016/j.jhydrol.2013.06.039, 2013.

Wong, J. S., Razavi, S., Bonsal, B. R., Wheater, H. S. and Asong, Z. E.: Evaluation of various daily precipitation products for large-scale hydro-climatic applications over Canada, Hydrol Earth Syst Sci Discuss, 2016, 1–

51, doi:10.5194/hess-2016-511, 2016.
Worqlul, A. W., Collick, A. S., Tilahun, S. A., Langan, S., Rientjes, T. H. M. and Steenhuis, T. S.: Comparing TRMM 3B42, CFSR and ground-based rainfall estimates as input for hydrological models, in data scarce regions: the Upper Blue Nile Basin, Ethiopia, Hydrol Earth Syst Sci Discuss, 2015, 2081–2112, doi:10.5194/hessd-12-2081-2015, 2015.
Xu, S., Wu, C., Wang, L., Gonsamo, A., Shen, Y. and Niu, Z.: A new satellite-based monthly precipitation downscaling algorithm with non-stationary relationship between precipitation and land surface characteristics, Remote Sens. Environ., 162, 119–140, doi:10.1016/j.rse.2015.02.024, 2015.
Zhou, L., Chen, Y., Liang, N. and Ni, Y.: Daily rainfall model to merge TRMM and ground based observations for rainfall estimations, in 2016 IEEE International Geoscience and Remote Sensing Symposium (IGARSS), pp. 601–604., 2016.

Table 1 Regression model performance and regression coefficients.

Year	Mean (mm)	R^2	E_{RMS} (mm)	E_{MAR} (%)	*a*	*b*	*c*
2001	961	0.91	138	10.6	3038.1	-345.3	359.8
2002	887	0.90	119	10.2	1354.7	687.5	212.0
2003	828	0.75	155	14.0	1700.2	-115.5	472.7
2004	1018	0.89	171	12.4	3784.3	-1047.7	517.4
2005	810	0.93	97	9.5	2465.4	-265.0	363.2
2006	737	0.88	122	11.4	2065.2	-112.2	287.5
2007	928	0.84	184	14.6	2306.9	53.5	286.4
2008	960	0.91	121	9.4	2504.0	-258.1	433.5
2009	726	0.89	119	13.2	2091.3	-168.0	294.5
2010	937	0.94	124	9.1	4094.8	-1293.3	512.6
2011	824	0.84	167	14.2	4697.8	-2613.7	792.7
2012	791	0.89	114	10.6	1966.4	3.5	308.1
RME	848	0.83	174	15.2	2670.4	-471.2	409.2

Table 2 Statistics of regression models for validation and calibration under three scenarios.

Scenario	Statistics	Calibration				Validation		
		R	R^2	E_{RMS} (mm)	E_{MAR} (%)	*R*	E_{RMS} （mm）	E_{MAR} (%)
a	mean	0.91	0.83	175	16.6	0.91	173.9	16.8
	max	0.92	0.85	186.2	17.8	0.94	211.8	19.9
	min	0.9	0.81	161.1	15.7	0.88	141	13.2
b	mean	0.92	0.84	166.6	15.8	0.91	186.1	17.8
	max	0.94	0.89	207	19.7	0.95	229.7	23.3
	min	0.89	0.8	126.2	12.8	0.89	148.6	12.9
c	mean	0.91	0.82	172.7	16.5	0.91	180.8	17.3
	max	0.95	0.91	207.9	19.1	0.94	204.8	24.4
	min	0.85	0.73	144.6	13.9	0.85	143.4	13.9

Table 3 Performance comparison between IDW, RME and TRMM

Method	Statistics	E_{RMS} (mm)	E_{MR}	E_{MAR}
IDW	max	273	0.1	0.26
	min	249	0.08	0.23
	mean	223	0.05	0.21
TRMM	max	220	0.17	0.24
	min	213	0.16	0.23
	mean	203	0.15	0.22
RME	max	183	0.07	0.18
	min	177	0.05	0.17
	mean	168	0.04	0.16
RME-IDW (%)	max	-32.9	-33	-30.5
	min	-26.3	-9.8	-21.4
	mean	-20.4	-1.2	-18.9
RME-TRMM (%)	max	-16.8	-59.5	-23.8
	min	-16.6	-66	-25.9
	mean	-17.4	-71.5	-28.3

Table 4 Regression model performance and coefficients of regression

	R^2	E_{RMS} (mm)	E_{MAR} (%)	a	b	c
NDVI	0.83	174.7	14.8	2670.4	-471.2	409.2
EVI	0.87	143.8	12.4	5129.6	702.5	254.7

Table 5 Results of two regression models established with extra independent variables: RME+T for temperature, RME+H for elevation

Model	R^2	E_{RMS} (mm)	E_{MAR} (%)	a	b	c	Extra b
RME	0.83	174.7	15	2670.4	-471.2	409.2	--
RME+T	0.84	172.6	15	2728.8	-496	407.3	-0.2
RME+H	0.84	172.6	15	2838.4	-638.7	492.9	-0.02

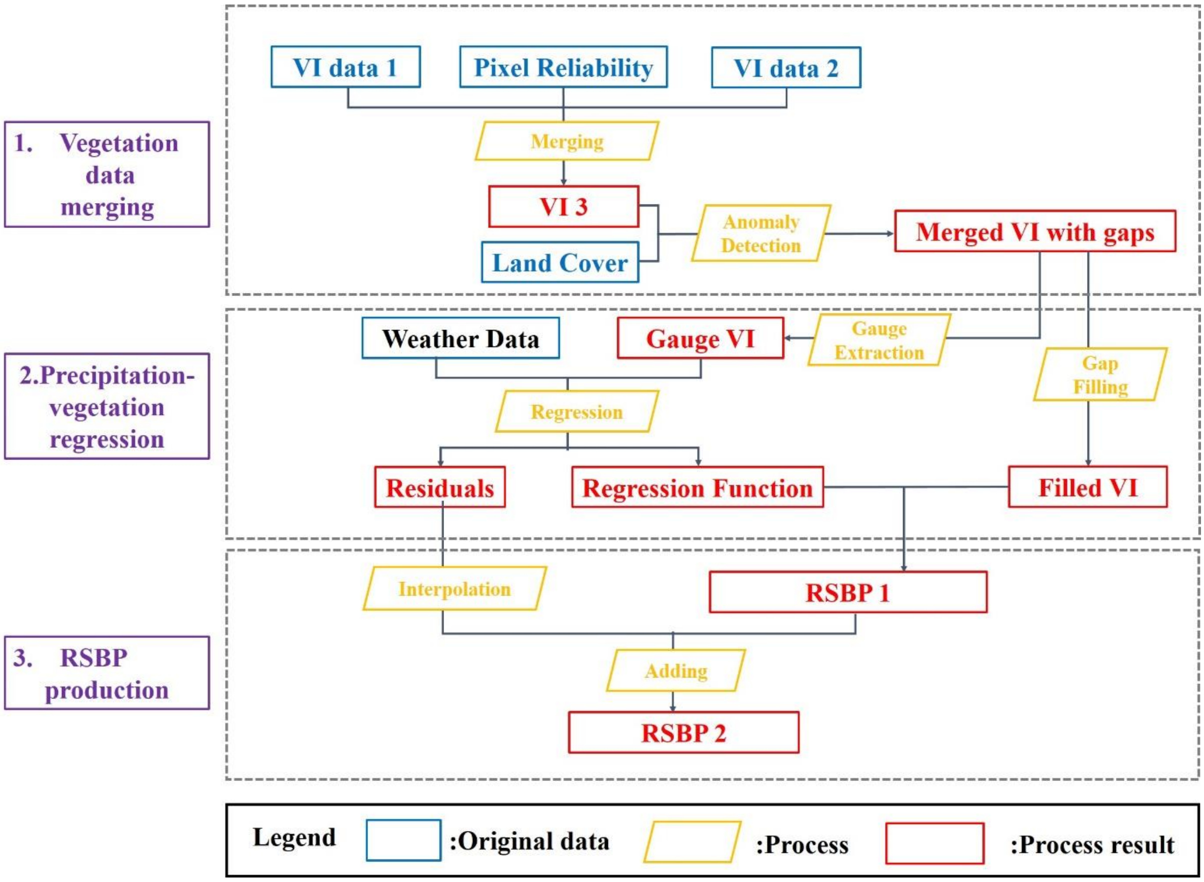

Figure 1 Flow chart of the satellite-gauge-vegetation fusion framework development.

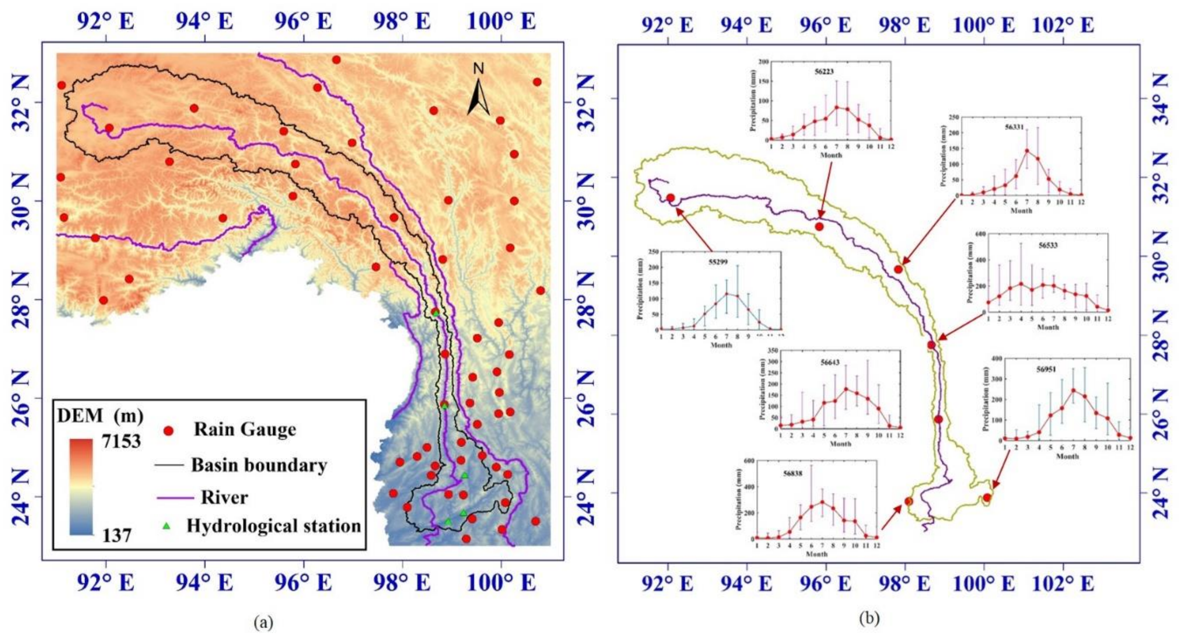

Figure 2 (a) Terrain map of the study area (the Nu-Salween basin and its adjacent areas); (b) The distribution of precipitation during the year across the Nu River.

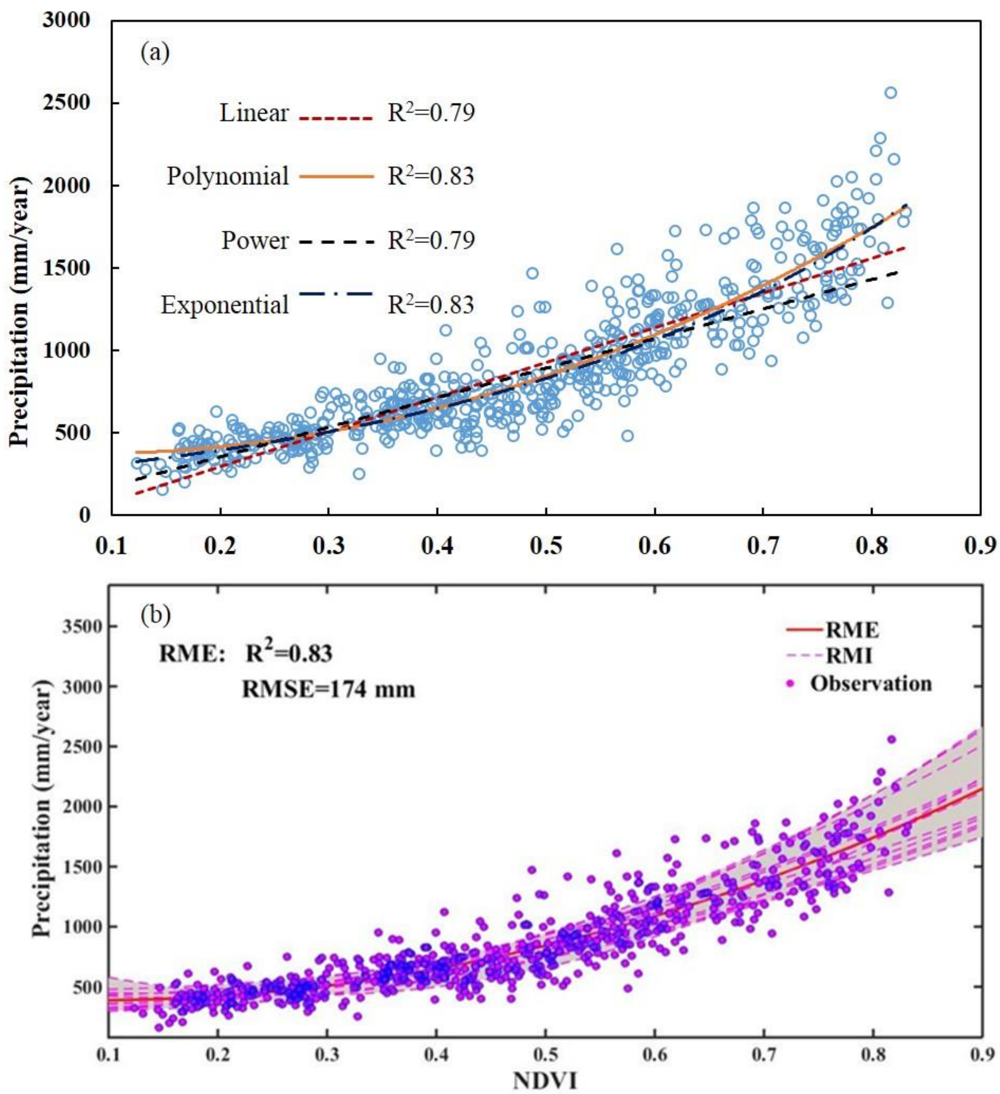

Figure 3 (a) Different regression forms for precipitation–NDVI relationship; (b) the precipitation-NDVI relationships for RME and RMI.

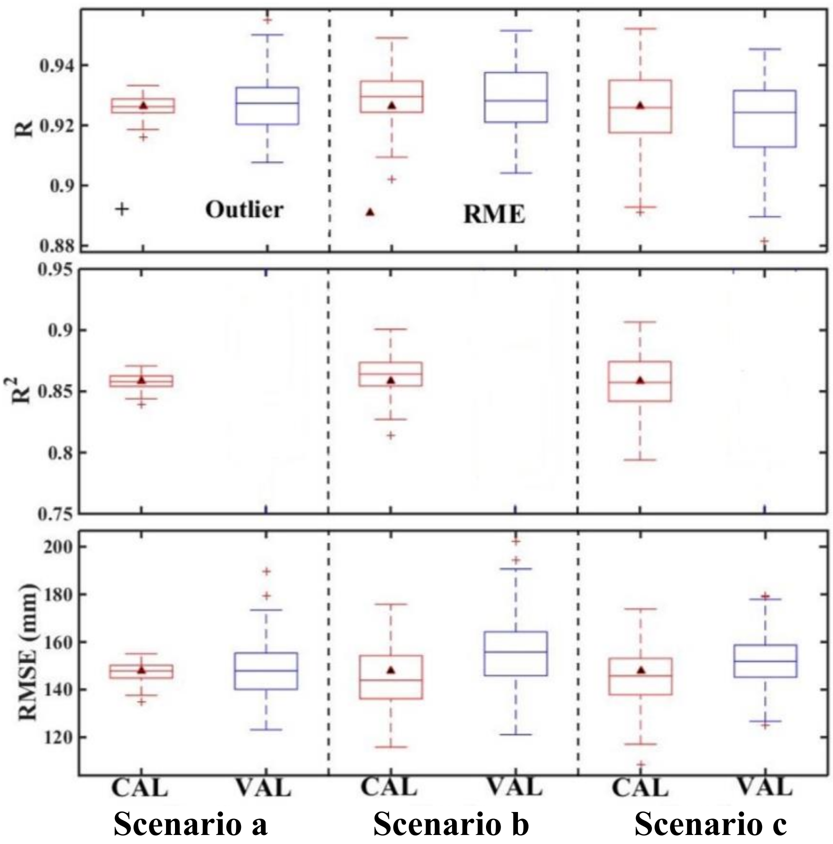

Figure 4 Box plots of R, R^2, E_{RMS} of RME model under three scenarios: a) fully random; b) all gauges, partial period; and c) partial gauges, entire period. Details of the three scenarios refer to Section 2.2. The triangle markers denote the value (R, R2 and RMSE) of RME model. The plus markers represent the outliers that are out of the range from (Q1-1.5IQR) to (Q3+1.5IQR). Q1 and Q3 are the 25th and 75th percentiles, and IQR (=Q3-Q1) is the interquartile range.

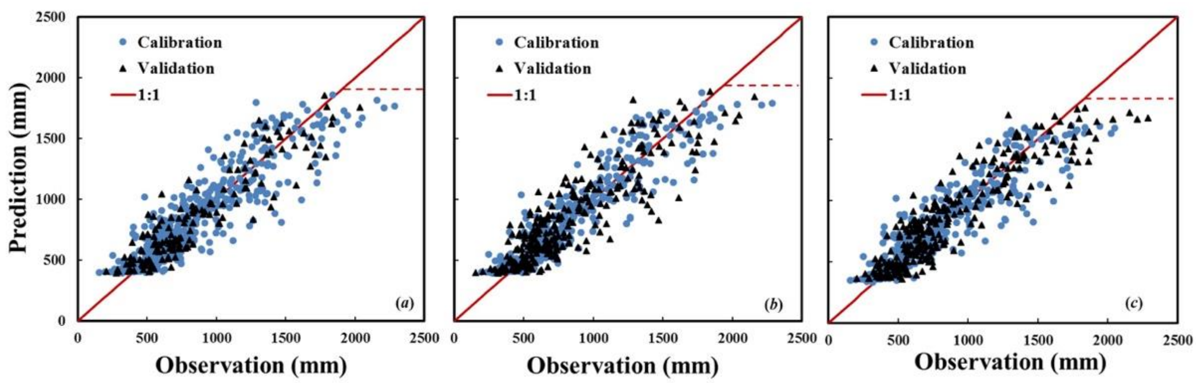

Figure 5 Comparison in annual precipitation between the gauged measurements and predictions by the regression model for scenario a) fully random; b) all gauges, partial period; and c) partial gauges, entire period. Details of the three scenarios refer to Section 2.2.

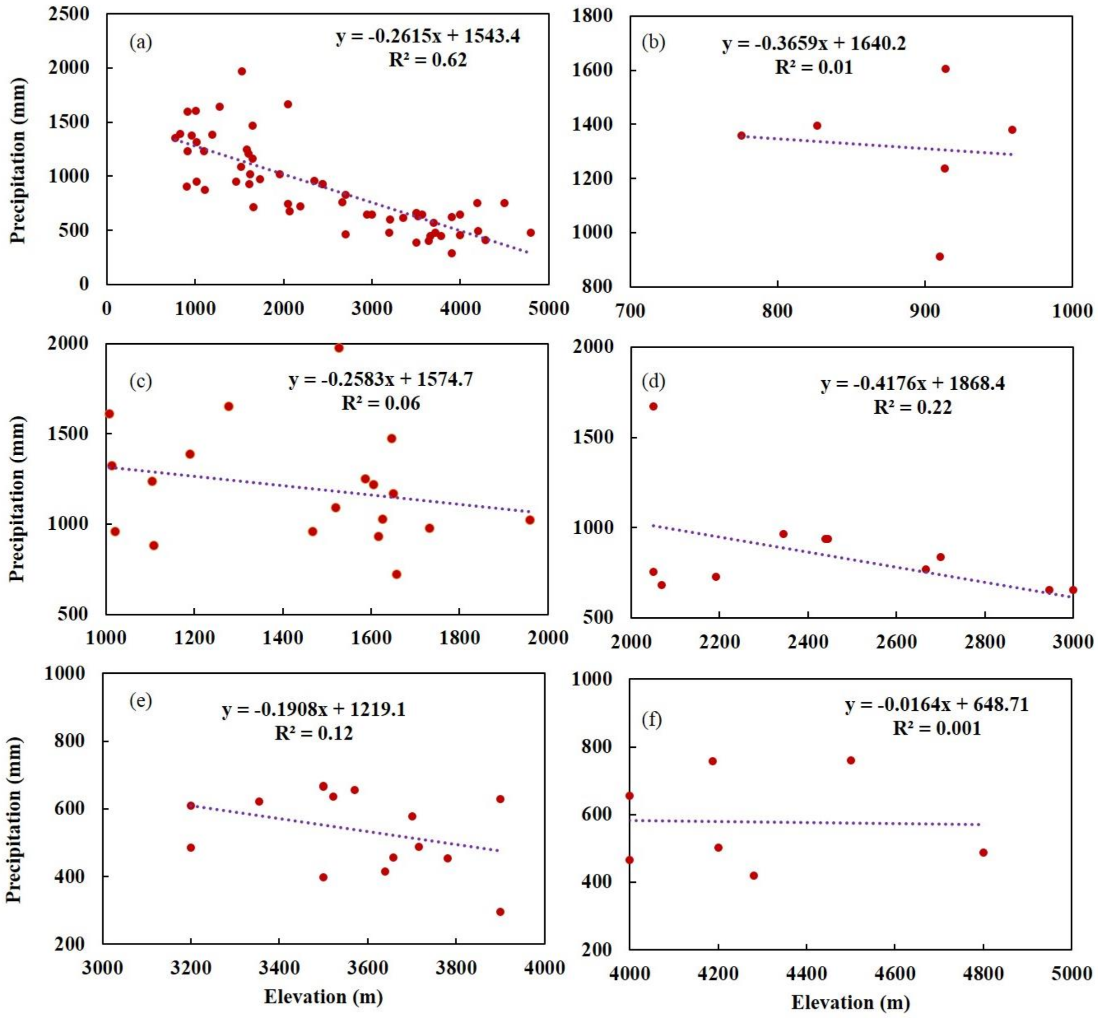

Figure 6 The mean annual precipitation-elevation relationships at different elevation bands, (a) whole elevation band; (b) elevation band :<1000 m; (c) band:1000~2000 m; (d) band: 2000~3000 m; (e) band :3000~4000 m; (f) band: >4000 m.

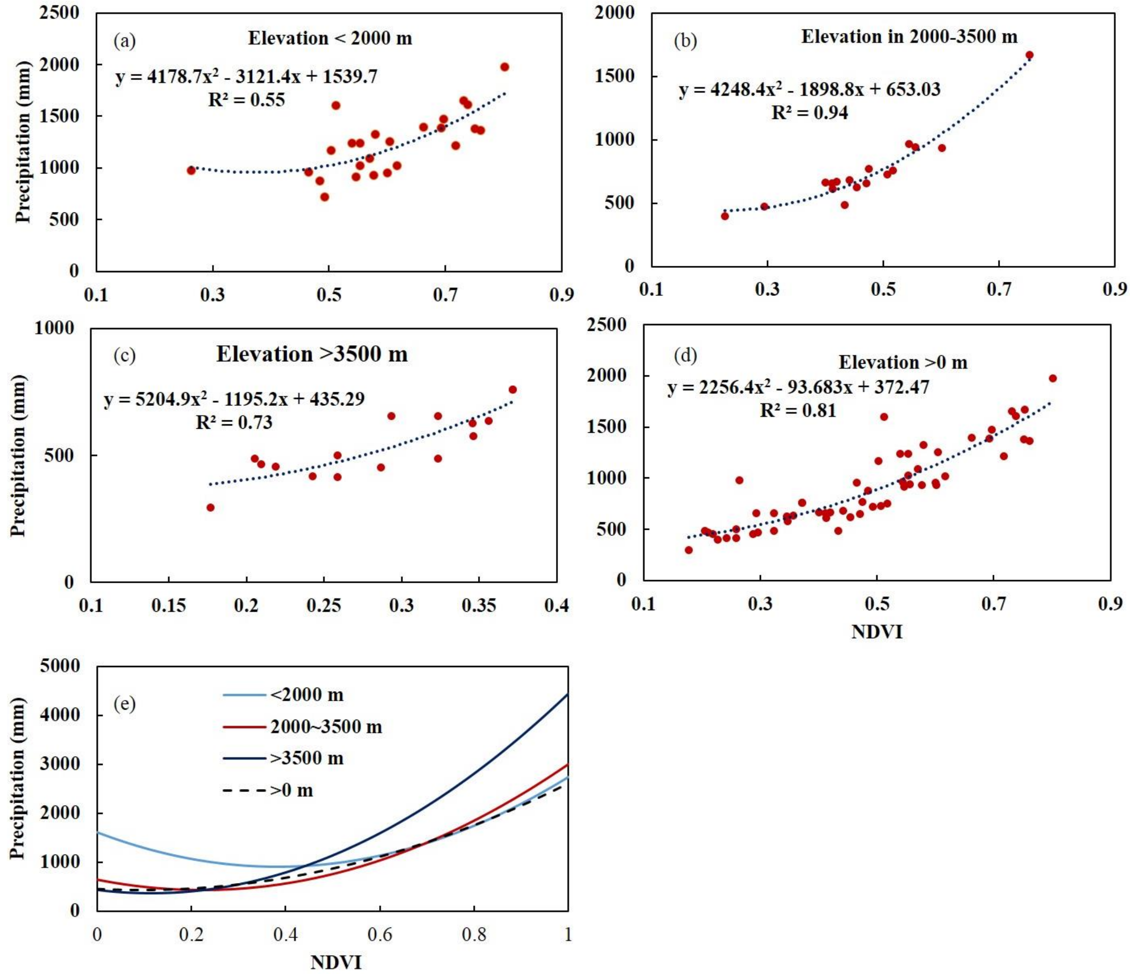

Figure 7 The mean annual precipitation-NDVI relationships at different elevation bands, (a) elevation band : <200 m; (b) band: 2000~3500 m; (c) band: >3500 m; (d) whole elevation band; (e) comparison of precipitation-NDVI relationship at different bands.

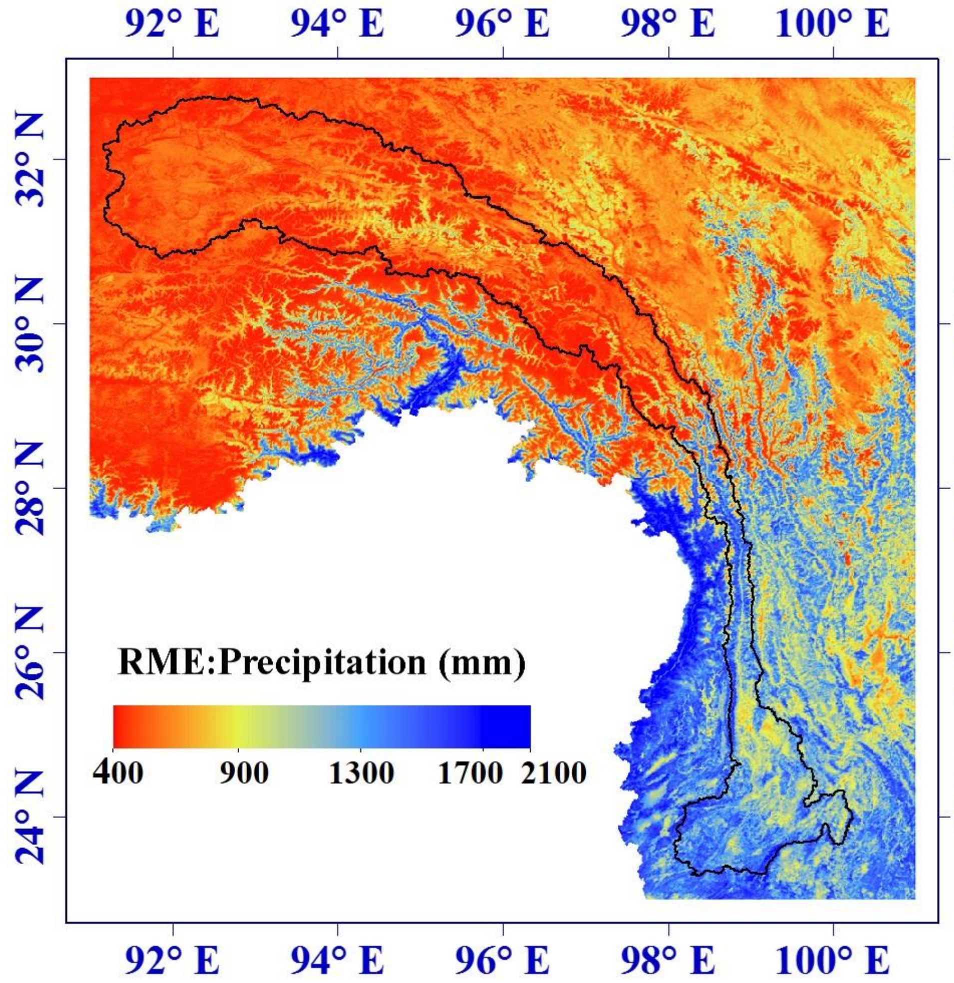

Figure 8 Average annual precipitation distribution of 2003-2012 from RME.

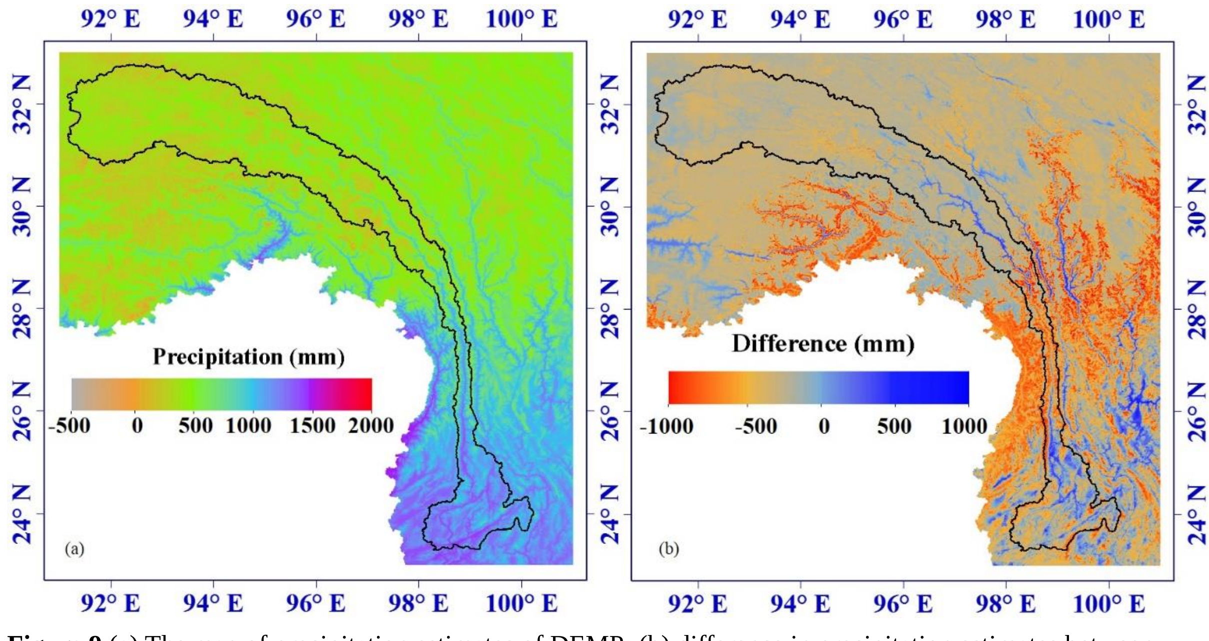

Figure 9 (a) The map of precipitation estimates of DEMP; (b) difference in precipitation estimates between RME and DEMP.

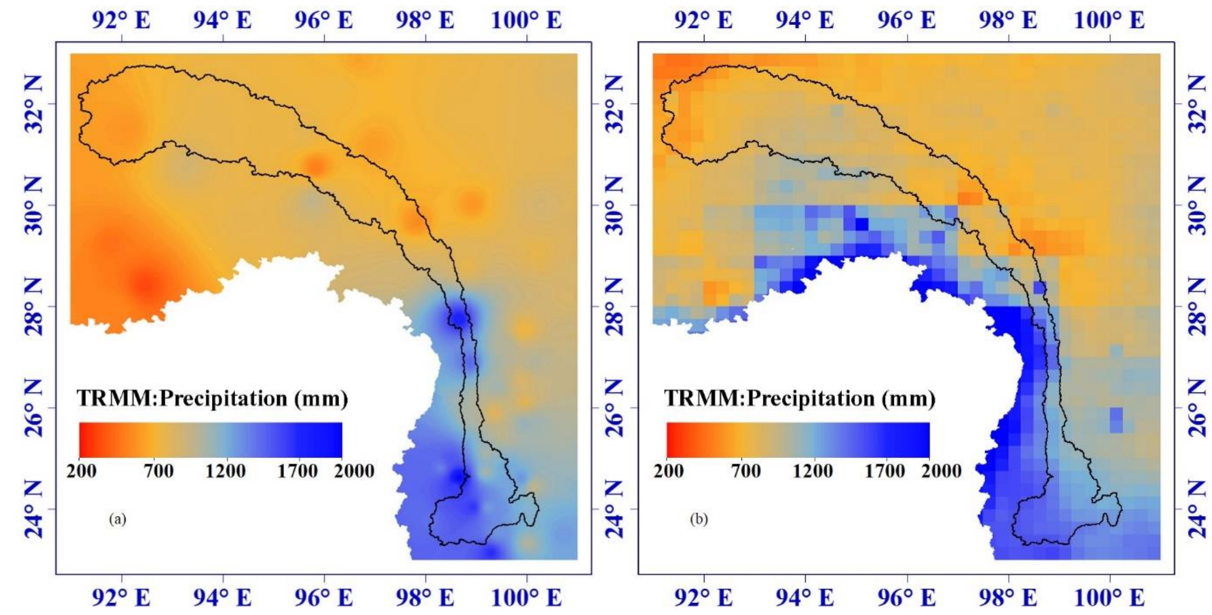

Figure 10 Spatial distribution of mean annual precipitation of 2003-2012 estimated by (a) IDW and (b) TRMM.

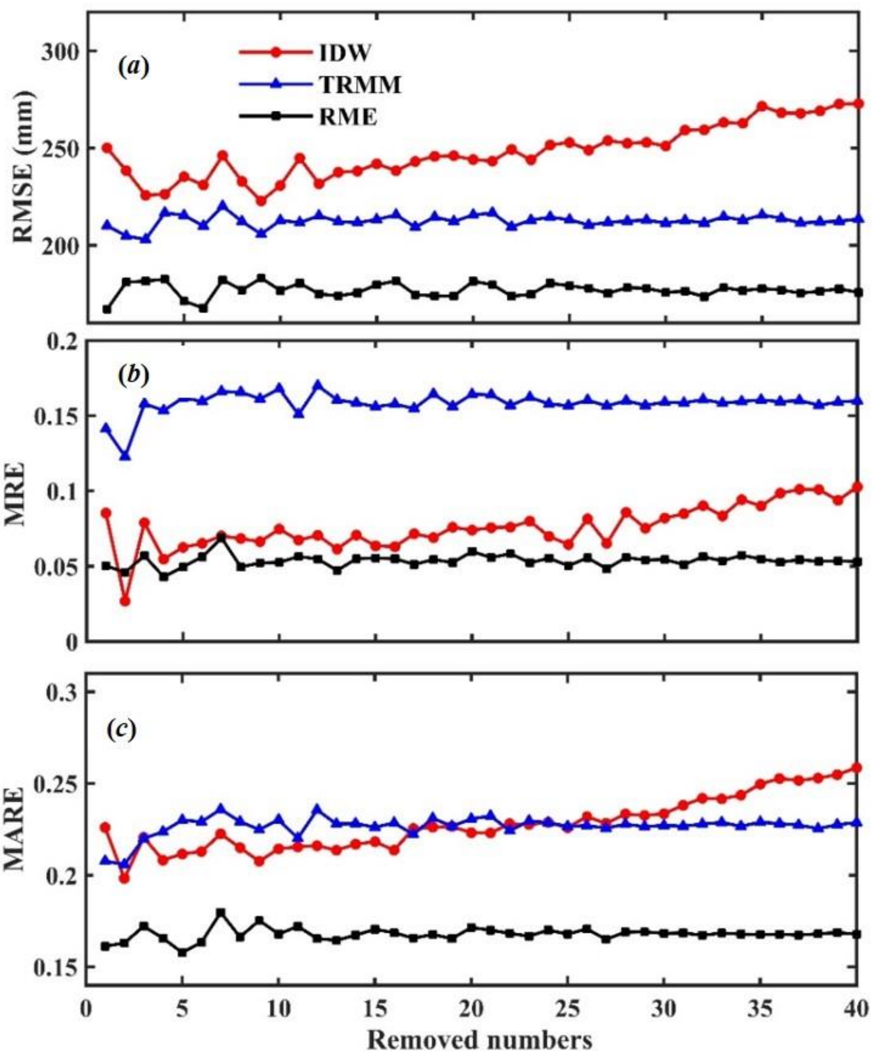

Figure 11 Performance of E_{RMS}, E_{MR} and E_{MAR} for three methods in different remove numbers.

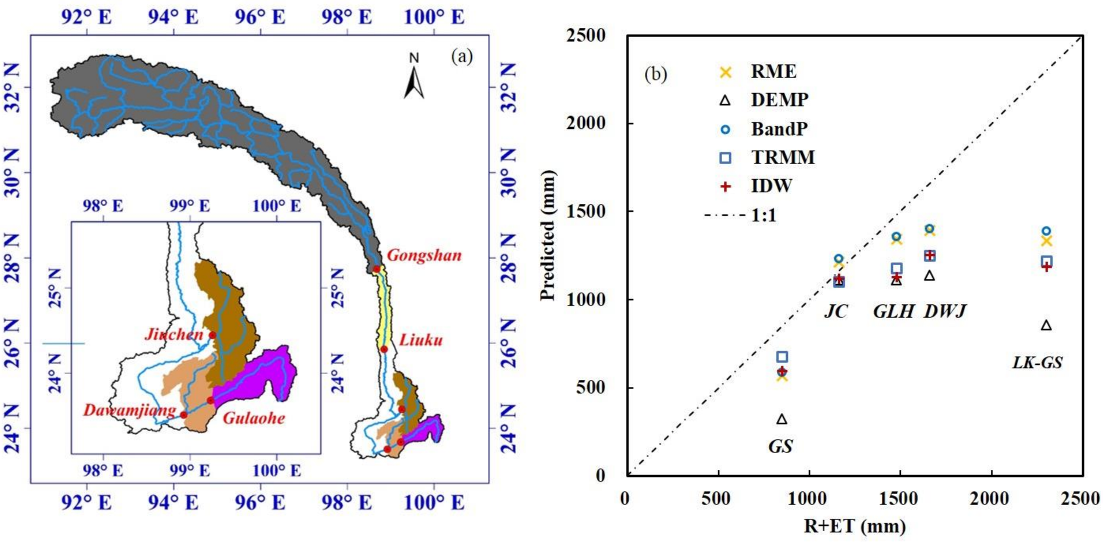

Figure 12 (a) Sub-basins based on hydrological stations (b) Comparison between water balance based precipitations (R+ET) and 5 precipitation products: DEMP (P-elevation relationship), BandP (P-NDVI relationship with consideration of elevation band), RME, TRMM and IDW. Here GS, JC, GLH, DWJ and LK-GS stand for Gongshan, Jiuchen, Gulaohe, Dawanjing and Liuku-Gongshan, respectively.

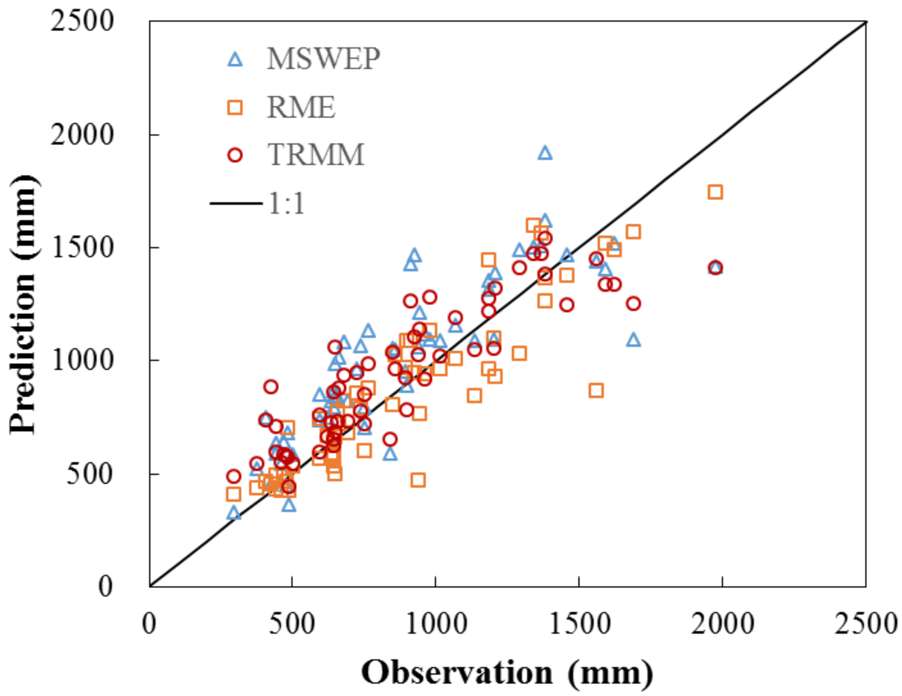

Figure 13 Comparison in mean annual precipitation between the gauged measurements and predictions by the MSWEP, RMM and RME.

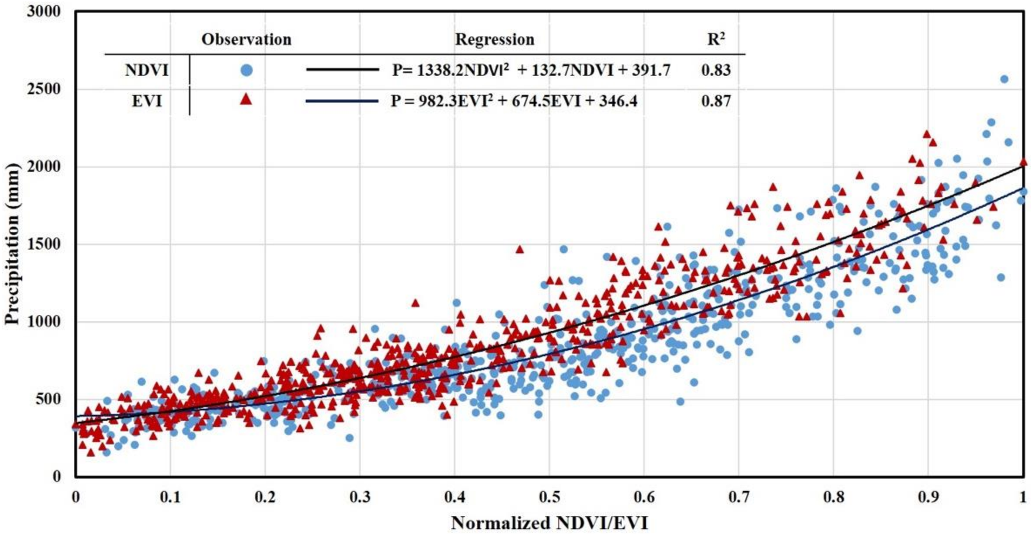

Figure 14 Regression relationship between annual precipitation and normalized NDVI/EVI

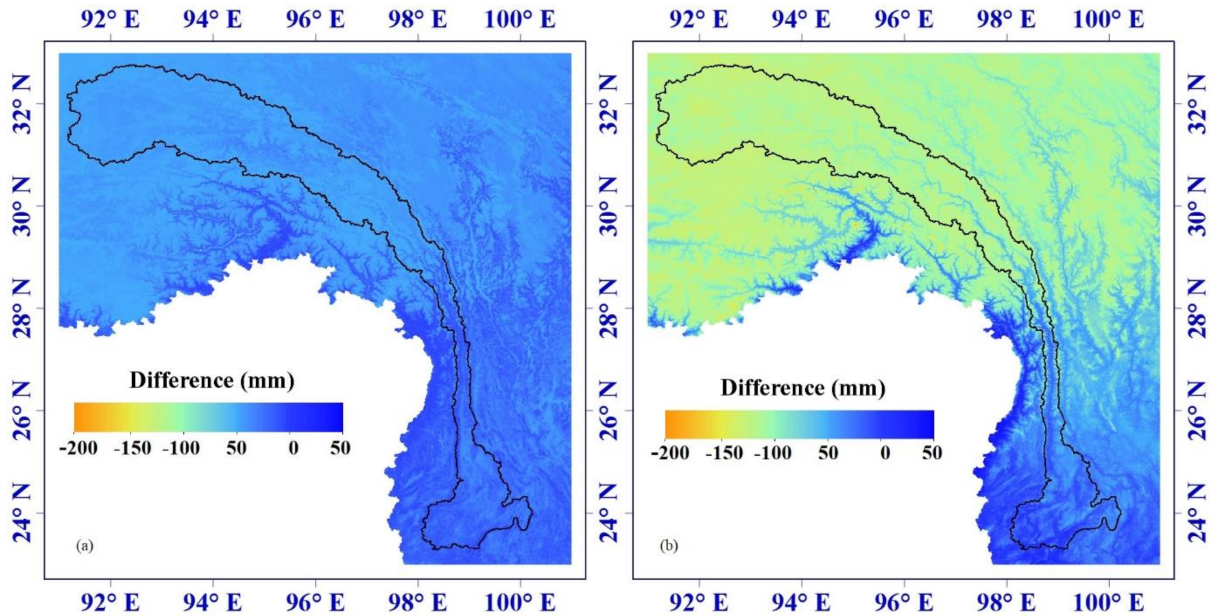

Figure 15 Spatial precipitation difference between RME and (a) RME+H; (b) RME+T.

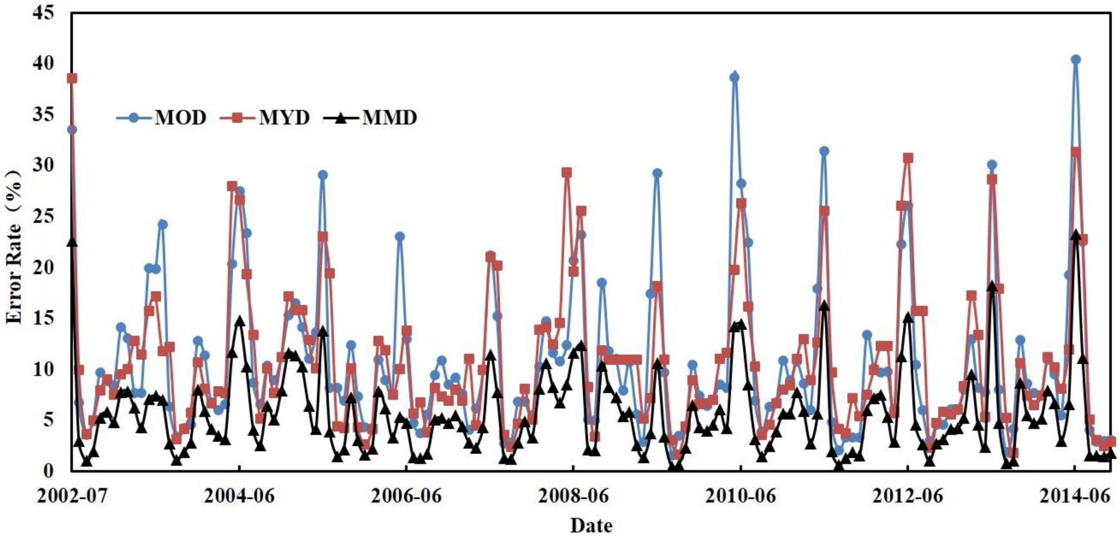

Figure A1 Monthly Error rate of MOD, MYD and MMD

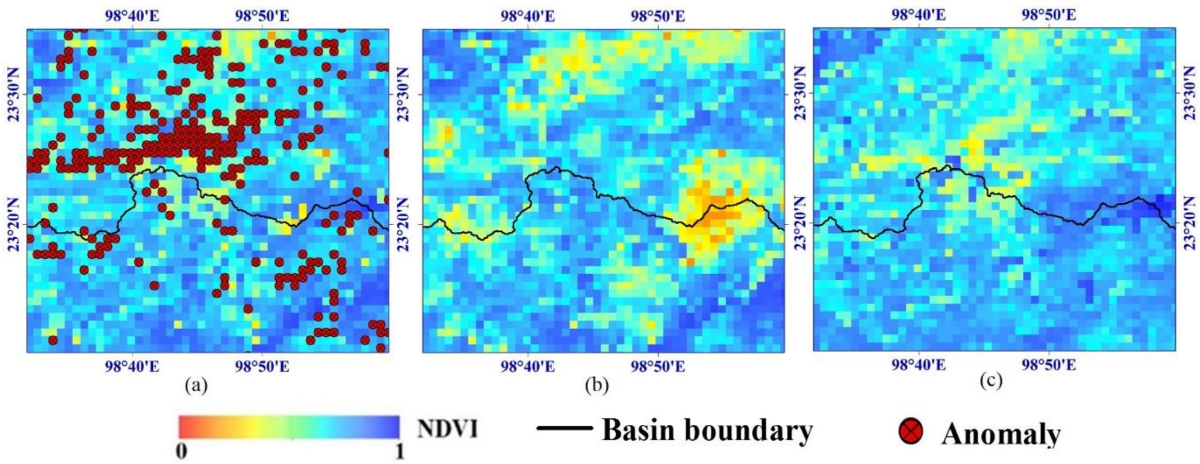

Figure A2 Comparison of three NDVI products over a ridge area on June 2006, (*a*) for MMD, (*b*) for MOD, (*c*) for MYD

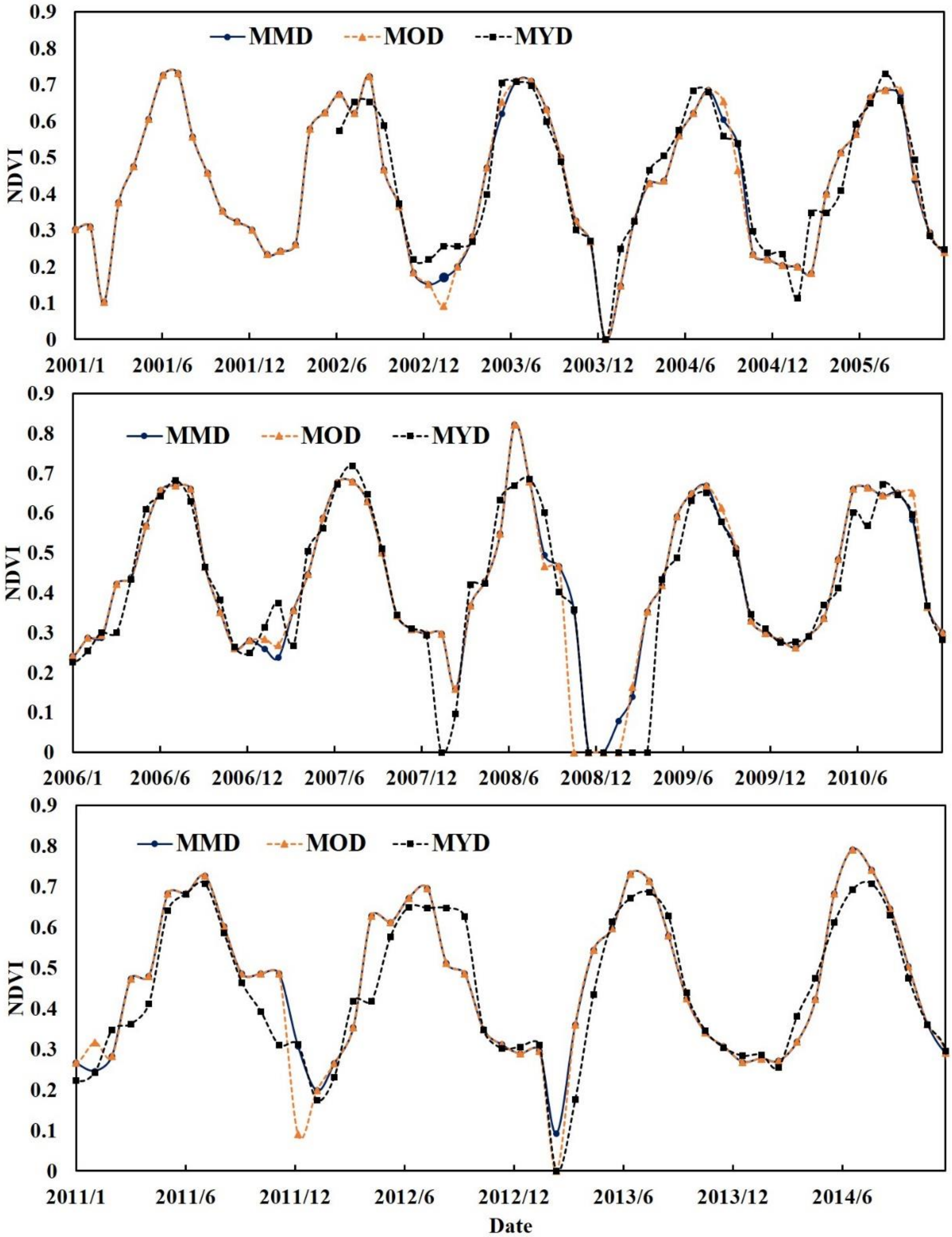

Figure A3 Comparison of three NDVI monthly time series over one gauge